Frontiers in Bioscience Landmark

Front. Biosci. (Landmark Ed) **2025**; 30(8): 39944
https://doi.org/10.31083/FBL39944

Original Research

MED10 as a Novel Oncogenic Driver in HCC: Promoting Cell Cycle Progression and Proliferation Through RAF1 Activation

Junhao Liu[1,2,†], Yongxue Lv[3,†], Kejun Liu[1,2], Zhengquan Li[1,2], Bendong Chen[1,2], Yang Bu[1,2,*]

[1]Department of Hepatobiliary Surgery, General Hospital of Ningxia Medical University, 750004 Yinchuan, Ningxia Hui Autonomous Region, China
[2]School of Clinical Medicine, Ningxia Medical University, 750004 Yinchuan, Ningxia Hui Autonomous Region, China
[3]School of Basic Medicine, Ningxia Medical University, 750004 Yinchuan, Ningxia Hui Autonomous Region, China
*Correspondence: boyang1976@163.com (Yang Bu)
[†]These authors contributed equally.

Academic Editor: Amancio Carnero Moya
Submitted: 24 April 2025 Revised: 13 July 2025 Accepted: 28 July 2025 Published: 29 August 2025

Abstract

Background: Mediator complex subunit 10 (MED10) serves as a critical regulator of eukaryotic gene expression by facilitating RNA polymerase II activity. Our investigation aims to characterize MED10's functional contributions and underlying molecular pathways in hepatocellular carcinoma (HCC) development. **Methods**: MED10 expression patterns in HCC and their correlation with clinicopathological parameters and patient outcomes were examined using bioinformatics databases and immunohistochemistry. Subsequently, we systematically investigated the biological functions of MED10 in the malignant progression of HCC through comprehensive *in vitro* experiments, including assessments of cell migration (transwell and wound healing assays), proliferative capacity (cell counting kit-8, colony formation, and 5-Ethynyl-2′-deoxyuridine assays), and cell cycle progression (flow cytometry analysis). Furthermore, we elucidated the underlying molecular mechanisms using real-time quantitative PCR (RT-qPCR), western blotting, immunofluorescence staining, and public database analyses. Furthermore, an *in vivo* subcutaneous xenograft model was employed to validate MED10's impact on tumor growth. **Results**: The results revealed a marked increase in MED10 expression levels within HCC tissues, showing a strong association with unfavorable clinical outcomes. Mechanistically, MED10 induced the epithelial-mesenchymal transition (EMT) and enhanced HCC cell migration. Moreover, MED10 overexpression drives HCC cell cycle progression and proliferation by activating rapidly accelerated fibrosarcoma 1 (RAF1), a process potentially mediated through the mitogen-activated protein kinase (MEK)/extracellular signal-regulated kinase (ERK)/cellular myelocytomatosis oncogene (c-Myc) signaling axis. **Conclusion**: MED10 promotes HCC cell migration and EMT but, more importantly, also drives cell cycle progression and proliferation via RAF1 activation, and is related to the MEK/ERK/c-Myc axis.

Keywords: hepatocellular carcinoma; mediator complex subunit 10; cell cycle; proliferation; MAPK signaling pathway; prognosis

1. Introduction

Hepatocellular carcinoma (HCC), the predominant type of primary liver cancer, ranks as the sixth most prevalent malignancy globally and accounts for the fourth highest mortality rate among cancer-related deaths [1]. According to projections made by the World Health Organization, HCC is anticipated to claim over one million lives annually by 2030, representing a growing global health crisis [2]. Due to its elusive early symptoms and heterogeneous nature, only a small proportion of patients with HCC are diagnosed sufficiently early to undergo radical resection, which is considered the preferred initial treatment [3]. Molecular-targeted therapies have transformed HCC management, yet their application remains restricted due to incomplete mechanistic insights [4]. This underscores the critical need to unravel HCC's molecular underpinnings.

Mediator complex subunit 10 (MED10) is a significant component of the mediator complex initially identified in yeast [5]. Functioning as an essential bridge connecting RNA polymerase II with transcription factors, the mediator complex serves as a master regulator of gene expression in eukaryotes [6]. This transcriptional control system governs fundamental biological phenomena ranging from cellular proliferation to organismal aging. Additionally, it critically influences pathological contexts, such as tumor cell metabolic activity and proliferation [7]. Structural or functional perturbations in mediator subunits typically reshape the transcriptional landscape of downstream effector genes, creating permissive conditions for malignant transformation and clinical disease evolution [8]. MED1 aggravates breast cancer by regulating macrophage M2 polarization [9]. MED12 mutations drive leiomyoma malignant progression through aberrant activation of the tryptophan/kynurenine/aryl hydrocarbon receptor signaling cascade [10]. Parallelly, in non-small cell lung cancer, tDR-007333-mediated AS-MED29 activation promotes aggressive tumor phenotypes [11]. In ER-positive breast cancer, MED16 regulates autophagy mediated by the mechanistic

target of rapamycin signaling pathway and promotes tumor progression and tamoxifen sensitivity [12]. Accumulating evidence supports MED10's pivotal contribution to oncogenesis. Aberrant MED10 expression has been shown to promote oncogenic and refractory phenotypes in bladder urothelial carcinoma, primarily through its regulation of hsa-miR-590. A recent study further demonstrated that MED10 enhances cisplatin resistance in HCC by facilitating phosphatase and tensin homolog (PTEN) ubiquitination [5,13]. These results position MED10 as a promising molecular target for HCC intervention strategies. However, the additional roles MED10 plays in HCC malignant progression and its underlying mechanisms require further exploration and validation, which may offer novel therapeutic targeting strategies for HCC treatment.

This study systematically investigated MED10's clinical significance and biological roles in HCC to discover innovative prognostic markers and therapeutic targets capable of revolutionizing HCC clinical practice. Our data establish MED10 upregulation in HCC tissues as a predictor of adverse clinical outcomes, mechanistically demonstrating its function as an oncogenic driver that promotes eithelial-mesenchymal transition (EMT) and metastatic competence. Importantly, further investigation indicated that MED10's influence on tumor cell proliferation and cell cycle progression was partly driven by aberrant activation of the rapidly accelerated fibrosarcoma 1 (RAF1). Together, these findings highlight MED10 as a potential dual-purpose biomarker for prognosis and a molecular target for HCC therapy.

2. Materials and Methods

2.1 Data Collection

RNA-seq data and associated clinical records for HCC (n = 374) and normal liver tissues (n = 50) were retrieved from The Cancer Genome Atlas (TCGA) database (https://portal.gdc.cancer.gov/). MED10 expression patterns across multiple tumor types were further evaluated using the TIMER2.0 platform (http://timer.cistrome.org/) [14].

2.2 Gene Set Enrichment Analysis (GSEA)

TCGA-LIHC patient data were stratified into high- and low-MED10 expression groups based on median expression values. GSEA was conducted using the clusterProfiler R package (version 4.10.0, https://bioconductor.org/packages/clusterProfiler/) to delineate functionally relevant pathways between these groups [15]. Statistical significance was defined as $p < 0.05$, with a false discovery rate threshold of <0.25 and a normalized enrichment score absolute value >1.

2.3 Functional Enrichment Analysis

Gene Ontology (GO) and Kyoto Encyclopedia of Genes and Genomes (KEGG) pathway analyses were performed using the Metascape platform (https://metascape.org/gp/index.html#/main/step1) [16].

2.4 Protein-protein Interaction Network (PPI)

To investigate potential functional associations, we generated a PPI network using the STRING database (https://cn.string-db.org/) by analyzing MED10 alongside cell cycle regulatory genes [17].

2.5 TRRUST, CHEA, ENCODE, and CHIP Atlas Databases

Target genes of the transcription factor, c-Myc, were predicted using the TRRUST (https://www.grnpedia.org/trrust/), CHEA (https://maayanlab.cloud/chea3/), ENCODE (https://www.encodeproject.org), and CHIP Atlas (https://chip-atlas.org/) databases [18–21]. Biological processes involved in c-Myc expression were predicted using the TRRUST database.

2.6 JASPAR Database

Bioinformatic analysis utilizing the JASPAR database (http://jaspar.genereg.net) [22] predicted the presence of c-Myc response elements within the promoter sequences of cyclin-dependent kinase 4 (CDK4), cyclin-dependent kinase 6 (CDK6), and cyclin D1 (CCND1).

2.7 Clinical Samples

This retrospective analysis utilized archived paraffin-embedded tissues and clinical records from 215 HCC patients who underwent surgical resection at Ningxia Medical University General Hospital between 2010–2020. The study cohort was selected based on strict inclusion criteria: (1) histologically confirmed HCC diagnosis, (2) treatment-naïve status prior to surgery, (3) availability of complete clinical datasets, and (4) paired tumor and normal liver tissue samples (collected >2 cm from tumor margins). Exclusion criteria: (1) combination with other malignant tumors; (2) combination with cardiovascular and respiratory disease. The study was carried out in accordance with the guidelines of the Declaration of Helsinki. The Institutional Review Board of Ningxia Medical University approved all protocols, and written informed consent was obtained from each participant prior to sample collection.

2.8 Antibodies

Antibodies against the following were used: p-RAF1 (9427, Cell Signaling Technology, Danvers, MA, USA), MED10 (DF13141, Affinity, Nanjing, Jiangsu, China), E-cadherin (60335-1-Ig, Proteintech, Wuhan, Hubei, China), p-ERK1/2 (AF1015, Affinity, Nanjing, Jiangsu, China), Cyclin D1 (ab16663, Abcam, Cambridge, Cambridgeshire, UK), RAF1 (ab181115, Abcam, Cambridge, Cambridgeshire, UK), MEK1/2 (9122, Cell Signaling Technology, Danvers, MA, USA), Vimentin (PA1-16759, Invitrogen, Carlsbad, CA, USA), ERK1/2 (11257-1-

AP, Proteintech, Wuhan, Hubei, China), CDK6 (ab222395, Abcam, Cambridge, Cambridgeshire, UK), matrix metallopeptidase 13 (MMP13, ab39012, Abcam, Cambridge, Cambridgeshire, UK), c-Myc (5605, Cell Signaling Technology, Danvers, MA, USA), N-cadherin (66219-1-Ig, Proteintech, Wuhan, Hubei, China), p-MEK1/2 (9154, Cell Signaling Technology, Danvers, MA, USA), CDK4 (ab108357, Abcam, Cambridge, Cambridgeshire, UK), marker of proliferation ki-67 (Ki67, 9027, Cell Signaling Technology, Danvers, MA, USA) and β-actin (ab213262, Abcam, Cambridgeshire, Cambridge, UK).

2.9 Immunohistochemistry (IHC)

Following dewaxing of the paraffin-embedded tissue sections in xylene, a graded alcohol series was used for rehydration. To expose target antigens, the sections were microwaved in sodium citrate buffer (C1010, Solarbio, Beijing, China). After cooling to room temperature, the samples were rinsed three times with phosphate-buffered saline (PBS, P1010, Solarbio, Beijing, China) and then treated with a peroxidase-blocking solution (PV-9001, ZSGB-BIO, Beijing, China) for 10 minutes. Subsequent PBS washes were performed before blocking nonspecific binding sites with 5% bovine serum albumin (BSA, SW3015, Solarbio, Beijing, China) for an additional 10 minutes. Primary antibody incubation was carried out overnight at 4 °C, followed by PBS washes and a 1-hour room-temperature incubation with secondary antibodies (PV-9001, ZSGB-BIO, Beijing, China). The primary antibodies used were as follows: MED10 (1:100, DF13141; Affinity, Nanjing, China), Ki67 (1:200, 9027, Cell Signaling Technology, Danvers, MA, USA). Following another PBS wash, the sections were developed using a 3,3'-Diaminobenzidine (DAB) kit (ZLI9018, ZSGB-BIO, Beijing, China), counterstained with hematoxylin (G1120, Solarbio, Beijing, China), dehydrated through an alcohol gradient, cleared in xylene, and finally mounted for microscopic imaging. Two independent pathologists assessed immunohistochemical staining, scoring both the proportion of positive cells (1–3) and staining intensity (0–4). The product of these scores yielded a composite value, with the median score serving as the threshold to classify samples into low- and high-expression groups.

2.10 Immunofluorescence (IF)

The tissue sections were first dewaxed in xylene and rehydrated using a graded alcohol series. Antigen retrieval was performed by heating the sections in sodium citrate buffer (C1010, Solarbio, Beijing, China). Afterward, the tissue sections were incubated with an endogenous peroxidase blocker (PV-9001, ZSGB-BIO, Beijing, China) for 10 minutes, followed by permeabilization with 0.3% Triton X-100 (T8200, Solarbio, Beijing, China) for 20 minutes. Nonspecific binding sites were then blocked with 5% BSA (SW3015, Solarbio, Beijing, China) for 1 hour. The sections were incubated with the primary antibody at 4 °C overnight, followed by a one-hour room-temperature incubation with a fluorescent secondary antibody. The primary antibodies used were as follows: MED10 (1:150, DF13141, Affinity, Nanjing, Jiangsu, China), CDK6 (1:150, ab222395, Abcam, Cambridge, UK), CDK4 (1:250, ab108357, Abcam, Cambridge, UK), Cyclin D1 (1:50, ab16663, Abcam, Cambridge, UK). Nuclei were counterstained with 4',6-diamidino-2-phenylindole (DAPI, C0065, Solarbio, Beijing, China), and the slides were mounted for imaging using an inverted fluorescence microscope (DMi8, Leica, Wetzlar, Hesse, Germany).

2.11 Cell Culture and Transfection

The human hepatoma cell lines MHCC97L, MHCC97H, HCCLM3, Hep3B, Huh-7, and SK-Hep-1, along with the immortalized hepatocyte line LO2, were kindly provided by the Institute of Liver Diseases at Fudan University (Shanghai, China). All cell lines were maintained in Dulbecco's modified Eagle medium (DMEM; VivaCell, Shanghai, China) supplemented with 10% fetal bovine serum (FBS, ExCell Bio, Shanghai, China) and 1% penicillin-streptomycin (P1400, Solarbio, Beijing, China) under standard culture conditions (37 °C, 5% CO_2). Prior to experimentation, cell line authenticity was confirmed through short tandem repeat (STR) profiling, and mycoplasma contamination testing yielded negative results.

For MED10 overexpression (ov-MED10 group), HCCLM3 cells were transduced with the lentiviral construct PDS279-PL-CMV-GFP-CC-DB-Puro-MED10, while control cells received the empty vector PDS279-pL-CMV-GFP-cc-dB-puro. MED10 knockdown (shMED10) was achieved using the lentiviral vector VP013-U6-MCS-CMV-ZsGreen-PGK-PURO-MED10-SHRNA, with the VP013-U6-MCS-CMV-ZsGreen-PGK-PURO vector serving as the shcontrol. All lentiviruses (Tsingke Biotech, Beijing, China) were transfected at 30–50% cell confluence using Lipo3000 (Invitrogen, Carlsbad, CA, USA) per manufacturer protocols. After 14 h, the viral medium was replaced with fresh complete medium. Transduced cells were selected with 2 µg/mL puromycin (P8230, Solarbio, Beijing, China) for 4–5 days, with transduction efficiency verified via green fluorescence microscopy. Where indicated, ov-MED10 cells were treated with 10 µM LY3009120 (S7842, Selleck Chemicals, Houston, TX, USA). MED10 targeting sequences are provided in **Supplementary Table 1**.

2.12 Real-Time Quantitative PCR (RT-qPCR)

Total RNA was isolated from cells using the MolarPure Cell/Tissue Total RNA Kit (19221ES, Yeasen Biotechnology, Shanghai, China). cDNA synthesis was performed with PrimeScript RT Master Mix (RR036A,

Takara Bio, Kyoto, Japan), followed by RT-qPCR analysis using TB Green Premix Ex Taq II (RR820A, Takara Bio, Kyoto, Japan) on a validated thermal cycler. Gene expression was calculated using the $2^{-\Delta\Delta Ct}$ method. The primers used to amplify these genes (Table 1) were designed and synthesized by Tsingke Biotech (Beijing, China).

Table 1. Primer sequences used for RT-qPCR.

Gene		Primer sequences (5′-3′)
MED10	Forward	GAGAAGTTTGACCACCTAGAGGA
	Reverse	TGGGGATTTCGACCTTGATCT
CDH1	Forward	ATTTTTCCCTCGACACCCGAT
	Reverse	TCCCAGGCGTAGACCA AGA
CDH2	Forward	AGCCAACCTTAACTGAGGAGT
	Reverse	GGCAAGTTGATTGGAGGGATG
VIM	Forward	AGTCCACTGAGTACCGGAGAC
	Reverse	CATTTCACGCATCTGGCGTTC
GAPDH	Forward	GGCAAATTCCATGGCACCGTCAAGG
	Reverse	GCCAGCATCGCCCCACTTGATTTTG

MED10, Mediator complex subunit 10; *CDH1*, Cadherin 1; *CDH2*, Cadherin 2; *VIM*, Vimentin; *GAPDH*, Glyceraldehyde-3-Phosphate Dehydrogenase.

2.13 Western Blotting

The total protein content was isolated from HCC tissues and cultured cells using radioimmunoprecipitation (RIPA) lysis buffer (P0013B, Beyotime Biotechnology, Shanghai, China) supplemented with protease inhibitors, phosphatase inhibitors, and phenylmethylsulfonyl fluoride (KGB5303-100, KeyGEN BioTECH, Nanjing, Jiangsu, China). After 20 min ice incubation, lysates were centrifuged (12,000 g, 10 min, 4 °C) to remove debris. Protein concentrations were quantified via bicinchoninic acid (BCA) assay (KGB2101-100, KeyGEN BioTECH, Nanjing, Jiangsu, China), followed by denaturation with loading buffer at 100 °C for 10 min. Samples were separated by sodium dodecyl sulfate-polyacrylamide gel electrophoresis (SDS-PAGE) and transferred to polyvinylidene fluoride (PVDF) membranes. Membranes were blocked for 1 h at room temperature with 5% BSA or skim milk, then incubated with primary antibodies overnight at 4 °C. The primary antibodies used were as follows: p-RAF1 (1:1000, 9427, Cell Signaling Technology, Danvers, MA, USA), MED10 (1:1500, DF13141, Affinity, Nanjing, Jiangsu, China), E-cadherin (1:2000, 60335-1-Ig, Proteintech, Wuhan, Hubei, China), p-ERK1/2 (1:2000, AF1015, Affinity, Nanjing, Jiangsu, China), Cyclin D1 (1:1000, ab16663; Abcam, Cambridge, Cambridgeshire, UK), RAF1 (1:1000, ab181115; Abcam, Cambridge, Cambridgeshire, UK), MEK1/2 (1:1000, 9122, Cell Signaling Technology, Danvers, MA, USA), Vimentin (1:1500, PA1-16759, Invitrogen, Carlsbad, CA, USA), ERK1/2 (1:3000, 11257-1-AP, Proteintech, Wuhan, Hubei, China), CDK6 (1:1000, ab222395, Abcam, Cambridge, Cambridgeshire, UK), MMP13 (1:2000, ab39012, Abcam, Cambridge, Cambridgeshire, UK), c-Myc (1:1000, 5605, Cell Signaling Technology, Danvers, MA, USA), N-cadherin (1:2000, 66219-1-Ig, Proteintech, Wuhan, Hubei, China), p-MEK1/2 (1:1000, 9154, Cell Signaling Technology, Danvers, MA, USA), CDK4 (1:1500, ab108357, Abcam, Cambridge, Cambridgeshire, UK), and β-actin (1:3000, ab213262, Abcam, Cambridge, Cambridgeshire, UK). Following three TBST (T1086, Solarbio, Beijing, China) washes, membranes were probed with Goat Anti-Rabbit IgG H&L (HRP) (1:5000, ab6721, Abcam, Cambridge, Cambridgeshire, UK) or Goat Anti-Mouse IgG H&L (HRP) (1:5000, ab205719, Abcam, Cambridge, Cambridgeshire, UK) for 1 h at room temperature. Protein bands were visualized using an enhanced chemiluminescence plus kit (PE0010, Solarbio, Beijing, China) with chemiluminescence imaging.

2.14 Transwell Assay

500 µL of DMEM supplemented with 10% FBS was placed in the lower chamber of a Costar Transwell system (Corning, New York, NY, USA), while the upper chamber received 200 µL of serum-free DMEM containing 8×10^4 cells. Following 48 h incubation, non-migratory cells on the upper membrane surface were removed by gentle swabbing. Migrated cells on the lower surface were fixed with 4% paraformaldehyde (15 min), stained with 0.1% crystal violet (30 min), and imaged using an inverted fluorescence microscope (DMi8, Leica, Wetzlar, Hesse, Germany). Cell counts were quantified from five random fields per membrane using ImageJ software (version 1.8.0, National Institutes of Health, Bethesda, MD, USA).

2.15 Wound-healing Assay

Confluent cell monolayers in 6-well plates were wounded using a sterile 200-µL pipette tip. After gentle PBS washing to remove debris, cells were maintained in serum-free medium. Wound closure was documented at 0 and 48 hours usingan inverted fluorescence microscope (DMi8, Leica, Wetzlar, Hesse, Germany).

2.16 Cell Proliferation Assay

Cell proliferation was assessed using the Cell Counting Kit-8 (CCK-8) assay (B34304; Biomake, Beijing, China). HCC cells (2000 cells/well) were seeded in 96-well plates and cultured at 37 °C. At designated timepoints (12, 24, 48, 72, 96 h), 10 µL CCK-8 reagent in 100 µL DMEM was added per well. Following 2 h incubation, absorbance at 450 nm was measured using a microplate reader, with background subtraction from control wells.

2.17 Colony Formation Assay

Cells were seeded in 6-well plates at 500 cells/well and cultured for 14 days. Resulting colonies were fixed with 4%

paraformaldehyde (15 min), PBS-washed, and stained with 0.1% crystal violet (30 min). Colony quantification was performed using ImageJ software (version 1.8.0, National Institutes of Health, Bethesda, MD, USA).

2.18 5-Ethynyl-2′-deoxyuridine (EdU) Assay

Cell proliferation was assessed using the BeyoClick™ EdU-555 Kit (C0075S; Beyotime, Shanghai, China). HCC cells grown in 24-well plates for 24 h were pulse-labeled with 10 µM EdU at 37 °C for 2 h. After fixation with 4% PFA (15 min) and permeabilization with 0.3% Triton X-100 (10 min), Click reaction solution was applied for 30 min in darkness. Nuclei were counterstained with Hoechst 33342 (5 min), and images acquired using an inverted fluorescence microscope (DMi8, Leica, Wetzlar, Hesse, Germany).

2.19 Cell Cycle Assay

HCC cells were harvested, washed in cold PBS, and centrifuged at 1000 ×g. After supernatant removal, pellets were fixed in 70% ethanol (4 °C, 12 h) and stained using a cell cycle analysis kit (C1052; Beyotime, Shanghai, China). DNA content was subsequently quantified via flow cytometry (ACEA Biosciences, San Diego, CA, USA).

2.20 Animal Experiments

Female BALB/c-nu nude mice (4–5-week-old) were sourced from Beijing Weitong Lihua Co., Ltd. (Beijing, China) and raised under standard conditions in a specific pathogen-free environment. Twenty-four nude mice were randomly divided into four experimental groups (6 mice/group): (1) control (injected with HCCLM3^{control} cells), (2) ov-MED10 (injected with HCCLM3$^{ov\text{-}MED10}$), (3) shcontrol (injected with Hep3B^{shcontrol}), and (4) shMED10 (injected with Hep3B^{shMED10}) groups. Subcutaneous xenograft tumors were established by injecting 150 µL of a cell suspension containing 5×10^6 respective HHC cells into the left axillary region of each mouse. On day 28 post-inoculation, all nude mice were anesthetized through intraperitoneal administration of sodium pentobarbital (3%, 50 mg/kg) and subsequently euthanized via cervical dislocation following confirmation of deep anesthesia. The volume of the removed tumor was measured, weighed, and photographed. Tumor volumes were calculated using the formula: volume = 0.5 × length × width^2. All animal experiments were conducted in accordance with protocols approved by the Medical Ethics Review Committee of Ningxia Medical University.

2.21 Statistical Analysis

Statistical analyses were performed using SPSS (version 26.0, IBM, Armonk, NY, USA) and GraphPad Prism (version 9.4.0, San Diego, Boston, MA, USA). Normally distributed continuous variables were compared between two groups with Student's *t*-test and among multiple groups with ANOVA. Associations between MED10 expression and clinicopathological features were evaluated using *t*-tests, Wilcoxon rank-sum, chi-square, or Fisher's exact tests. Survival curves were generated by Kaplan-Meier analysis with log-rank testing. MED10's diagnostic utility was assessed through receiver operating characteristic (ROC) curve analysis, while Cox proportional hazards regression identified survival predictors. A MED10-based prognostic nomogram was developed and validated using calibration curves. Statistical significance was defined as $p < 0.05$.

3. Results

3.1 MED10 is Significantly Overexpressed in HCC Tissues, Which is Related to the Poor Prognosis of Patients With HCC

Initial analysis of MED10 expression across multiple cancers using TIMER2.0 revealed significant upregulation in tumor tissues, particularly hepatocellular carcinoma (HCC), versus normal counterparts (Fig. 1A). TCGA database analysis further confirmed elevated MED10 expression in HCC tissues relative to both paired and unpaired adjacent normal liver samples (Fig. 1B,C). ROC curve assessment demonstrated strong diagnostic potential for HCC (area under the curve (AUC) = 0.897, Fig. 1D). Analysis of MED10's clinical relevance in HCC demonstrated significant correlations between its expression and key clinicopathological features, including body mass index, alpha-fetoprotein (AFP) levels, T stage, histologic grade, and vascular invasion (Table 2). Kaplan-Meier analysis demonstrated markedly inferior overall survival (OS), disease-specific survival (DSS), and progression-free interval (PFI) in HCC patients with elevated MED10 expression compared to low-expression cohorts (Fig. 1E–G). Univariate and multivariate Cox regression analyses consistently established MED10 as an independent prognostic determinant (Fig. 1H,I). We subsequently developed a clinical nomogram incorporating MED10 expression with eight clinicopathological parameters—gender, age, Child-Pugh grade, AFP level, T stage, histologic grade, pathologic stage, and vascular invasion—to predict 1-, 3-, and 5-year OS probabilities (Fig. 1J). The model's precision was validated through calibration curves showing exceptional concordance between predicted and observed survival rates across all timepoints (Fig. 1K), collectively confirming MED10's clinical utility as a prognostic biomarker.

This retrospective study validated public database findings through experimental analysis. IHC confirmed significantly elevated MED10 expression in HCC versus adjacent liver tissues (Fig. 1L–N). Western blotting corroborated these results, demonstrating increased MED10 levels in HCC specimens consistent with TCGA data (Fig. 1L–N). Among 215 HCC cases stratified by median immunohistochemistry scores, high MED10 expression correlated significantly with elevated aspartate aminotransferase levels, larger tumor size, microvascular tumor thrombi, and ad-

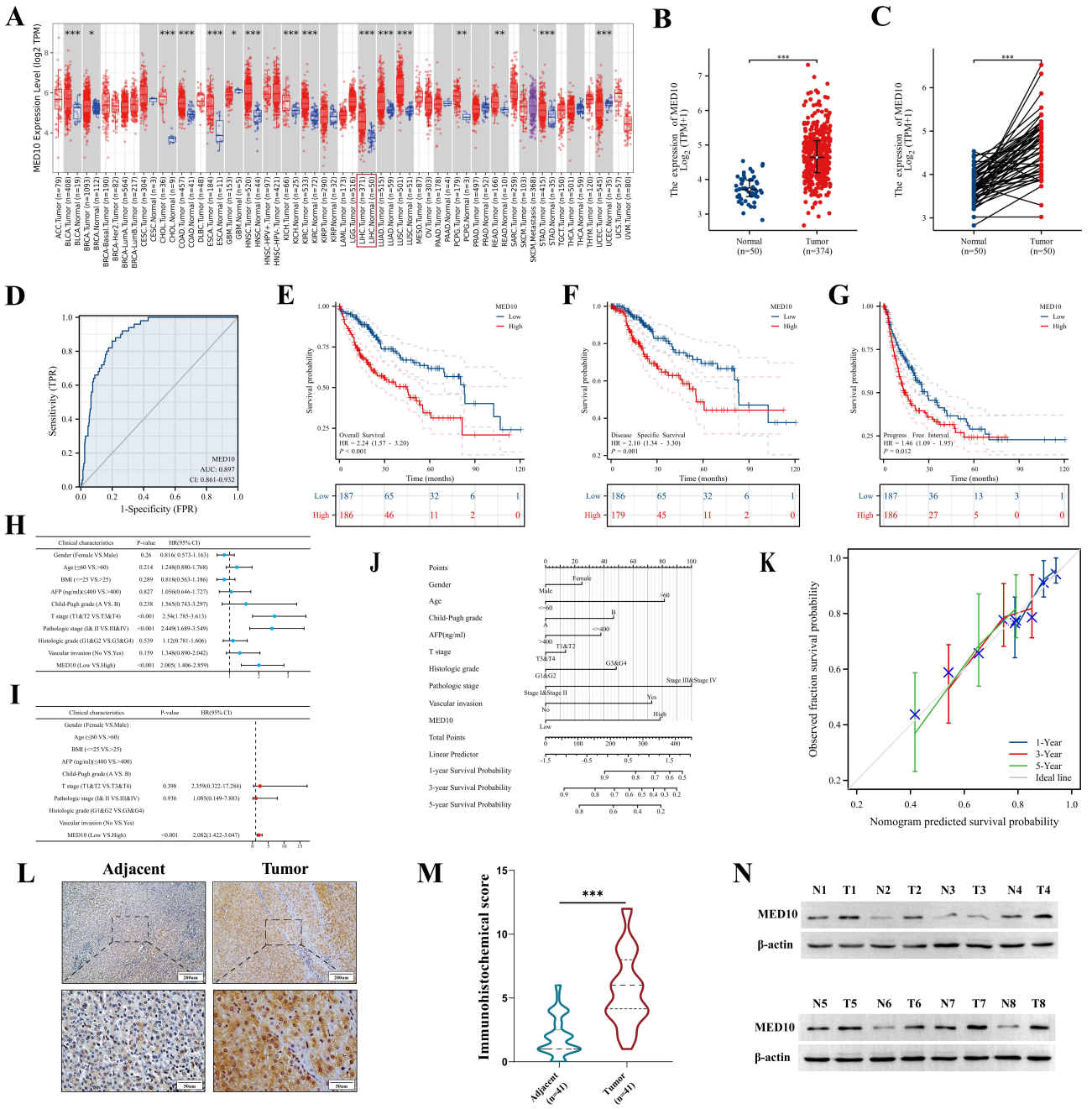

Fig. 1. MED10 overexpression in HCC correlates with poor prognosis. (A) Expression levels of MED10 across pan-cancer. The red box indicates higher expression of MED10 in liver hepatocellular carcinoma (LIHC) compared to adjacent normal tissues. (B,C) Elevated MED10 in HCC versus adjacent normal liver tissues. (D) Diagnostic receiver operating characteristic (ROC) curve for MED10 in HCC (area under the curve (AUC) = 0.897). (E–G) Survival analyses showing reduced overall survival (OS), disease-specific survival (DSS), and progression-free interval (PFI) in high-MED10 expressors. (H,I) Univariate and multivariate Cox regressions identifying MED10 as independent prognostic factor. (J) Prognostic nomogram predicting 1-/3-/5-year OS. (K) Nomogram calibration curves. (L) Representative Immunohistochemistry (IHC) of MED10 in HCC and normal tissues. Scale bars: 200 μm (top) and 50 μm (bottom). (M) Quantitative IHC scoring in 41 paired samples. (N) Western blotting confirmation of MED10 overexpression. *$p < 0.05$; **$p < 0.01$; ***$p < 0.001$.

vanced T stage (Table 3). These findings establish MED10 as a key pathogenic driver in HCC, where overexpression predicts aggressive disease and poor prognosis.

3.2 MED10 Drives EMT and Accelerates Migration in HCC Cells

Analysis of TCGA data and clinical cohorts identified significant associations between elevated MED10

Table 2. Association of MED10 expression with clinicopathological characteristics in TCGA HCC patients.

Characteristics	Expression of MED10		Statistic	*p*-value	Method
	Low (n = 187)	High (n = 187)			
Gender, n (%)			0.110	0.740	Chisq test
Female	62 (16.6%)	59 (15.8%)			
Male	125 (33.4%)	128 (34.2%)			
Age, n (%)			1.298	0.255	Chisq test
≤60	83 (22.2%)	94 (25.1%)			
>60	104 (27.8%)	93 (24.9%)			
BMI, n (%)			5.567	0.018	Chisq test
≤25	79 (23.4%)	98 (29.1%)			
>25	92 (27.3%)	68 (20.2%)			
AFP (ng/mL), n (%)			17.129	<0.001	Chisq test
≤400	129 (46.1%)	86 (30.7%)			
>400	20 (7.1%)	45 (16.1%)			
Child-Pugh grade, n (%)				0.904	Fisher test
A	116 (48.1%)	103 (42.7%)			
B	12 (5.0%)	9 (3.7%)			
C	1 (0.4%)	0 (0.0%)			
Fibrosis ishak score, n (%)			6.076	0.108	Chisq test
0	49 (22.8%)	26 (12.1%)			
1/2	16 (7.4%)	15 (7.0%)			
3/4	11 (5.1%)	17 (7.9%)			
5/6	45 (20.9%)	36 (16.7%)			
Pathologic T stage, n (%)			7.942	0.047	Chisq test
T1	104 (28%)	79 (21.3%)			
T2	42 (11.3%)	53 (14.3%)			
T3	32 (8.6%)	48 (12.9%)			
T4	6 (1.6%)	7 (1.9%)			
Histologic grade, n (%)			15.254	0.002	Chisq test
G1	37 (10.0%)	18 (4.9%)			
G2	96 (26.0%)	82 (22.2%)			
G3	47 (12.7%)	77 (20.9%)			
G4	5 (1.4%)	7 (1.9%)			
Pathologic stage, n (%)			7.210	0.066	Yates' correction
Stage I	98 (28%)	75 (21.4%)			
Stage II	40 (11.4%)	47 (13.4%)			
Stage III	34 (9.7%)	51 (14.6%)			
Stage IV	2 (0.6%)	3 (0.9%)			
Vascular invasion, n (%)			4.284	0.038	Chisq test
No	118 (37.1%)	90 (28.3%)			
Yes	49 (15.4%)	61 (19.2%)			

TCGA, The Cancer Genome Atlas; HCC, hepatocellular carcinoma; BMI, body mass index; AFP, alpha-fetoprotein.

expression and microvascular invasion/tumor thrombi in HCC patients (Tables 2,3). GSEA revealed marked enrichment of cell migration and EMT pathways in high-MED10 expressors (Fig. 2A), implicating MED10 in metastatic progression. Supporting this observation, both transcriptional and translational analyses revealed MED10 dysregulation in HCC cell lines (MHCC97L, MHCC97H, SK-Hep-1, Hep3B), showing significantly elevated mRNA and protein expression relative to normal hepatocytes (LO2) (Fig. 2B,C). To functionally characterize MED10, we engineered stable HCC cell lines with modulated expression: MED10 was overexpressed in low-expressing HCCLM3 cells and knocked down in high-expressing Hep3B cells. Successful overexpression (ov-MED10) and knockdown (shMED10) were validated by RT-qPCR and Western blotting (Fig. 2D,E). Functional assessments via Transwell and scratch assays established MED10's pro-migratory role in HCC: forced expression accelerated cel-

Table 3. Association of MED10 expression with clinicopathological characteristics in HCC clinical cohorts.

Characteristics	Expression of MED10		Statistic	*p*-value	Method
	High (n = 107)	Low (n = 108)			
Age (years), mean ± sd	54.5 ± 10.8	55.9 ± 11.3	–0.911	0.363	*T* test
Gender, n (%)			0.015	0.903	Chisq test
Male	82 (50.0%)	82 (50.0%)			
Female	25 (49.0%)	26 (51.0%)			
HBsAg, n (%)			0.030	0.863	Chisq test
Positive	93 (50.0%)	93 (50.0%)			
Negative	14 (48.3%)	15 (51.7%)			
WBC ($\times 10^9$/L), median (IQR)	5.2 (4.3, 6.3)	5.1 (4.2, 6.4)		0.992	Wilcoxon
NE ($\times 10^9$/L), median (IQR)	56.4 (49.3, 64.7)	54.4 (48.6, 63.4)		0.308	Wilcoxon
Lym ($\times 10^9$/L), mean ± sd	31.1 ± 10.6	31.9 ± 9.5	–0.589	0.557	*T* test
Hb (g/L), median (IQR)	144 (133.5, 157.0)	149 (134.5, 158.0)		0.338	Wilcoxon
PLT ($\times 10^9$/L), median (IQR)	166 (119.0, 210.0)	151 (120.3, 193.0)		0.425	Wilcoxon
AFP (ng/mL), n (%)			2.235	0.135	Chisq test
≥400	72 (53.7%)	62 (46.3%)			
<400	35 (43.2%)	46 (56.8%)			
ALB (ng/mL), median (IQR)	38.2 (36.0, 41.3)	38.6 (35.0, 41.6)		0.755	Wilcoxon
AST (ng/mL), median (IQR)	36.2 (28.7, 54.1)	29 (23.5, 45.8)		0.024	Wilcoxon
PT (S), median (IQR)	12.1 (11.4, 13.2)	12.2 (11.6, 13.4)		0.562	Wilcoxon
Tumor size (cm), n (%)			25.213	<0.001	Chisq test
≥5	64 (69.6%)	28 (30.4%)			
<5	43 (35.0%)	80 (65.0%)			
Microvascular tumor thrombus, n (%)			35.747	<0.001	Chisq test
Yes	68 (73.1%)	25 (26.9%)			
No	39 (32.0%)	83 (68.0%)			
Degree of differentiation, n (%)			1.118	0.572	Chisq test
Low	40 (54.8%)	33 (45.2%)			
Middle	49 (46.8%)	55 (53.6%)			
High	18 (47.4%)	20 (52.6%)			
T stage, n (%)			20.452	<0.001	Yates' correction
T1	8 (22.2%)	28 (77.8%)			
T2	53 (48.2%)	57 (51.8%)			
T3	44 (68.8%)	20 (31.2%)			
T4	2 (40.0%)	3 (60.0%)			

HBsAg, Hepatitis B Surface Antigen; WBC, White Blood Cell; NE, Neutrophil; Lym, Lymphocyte; Hb, Hemoglobin; PLT, Platelet; ALB, Albumin; AST, Aspartate Aminotransferase; PT, Prothrombin Time.

lular motility, whereas genetic ablation attenuated migration (Fig. 2F,G). To investigate MED10's role in EMT, we assessed EMT marker expression via RT-qPCR and Western blotting. MED10 overexpression elevated mesenchymal markers (N-cadherin, vimentin) while suppressing the epithelial marker E-cadherin. Conversely, MED10 knockdown increased E-cadherin and reduced mesenchymal markers (Fig. 2H,I). Protein levels of the metastatic regulator MMP13 mirrored these changes, increasing with MED10 overexpression and decreasing upon knockdown.

3.3 MED10 Promotes the Proliferation of HCC Cells In Vitro

Analysis of TCGA data and HCC clinical cohorts revealed significant correlations between MED10 expression and advanced T stage/tumor size (Tables 2,3). Building on these clinical associations, we investigated MED10's functional role in proliferation. Colony formation, CCK-8, and EdU assays consistently demonstrated enhanced proliferative capacity upon MED10 overexpression, whereas MED10 knockdown markedly suppressed HCC cell growth (Fig. 3A–C). To validate these findings *in vivo*, nude mouse xenograft models showed significantly reduced tumor burden in shMED10 groups versus controls, while ov-MED10 xenografts exhibited increased tumor volume and mass (Fig. 3D–F). IHC analysis of proliferation marker Ki-67 further confirmed these effects: diminished staining in shMED10 tumors and intensified staining in ov-MED10 tumors compared to respective controls (Fig. 3G).

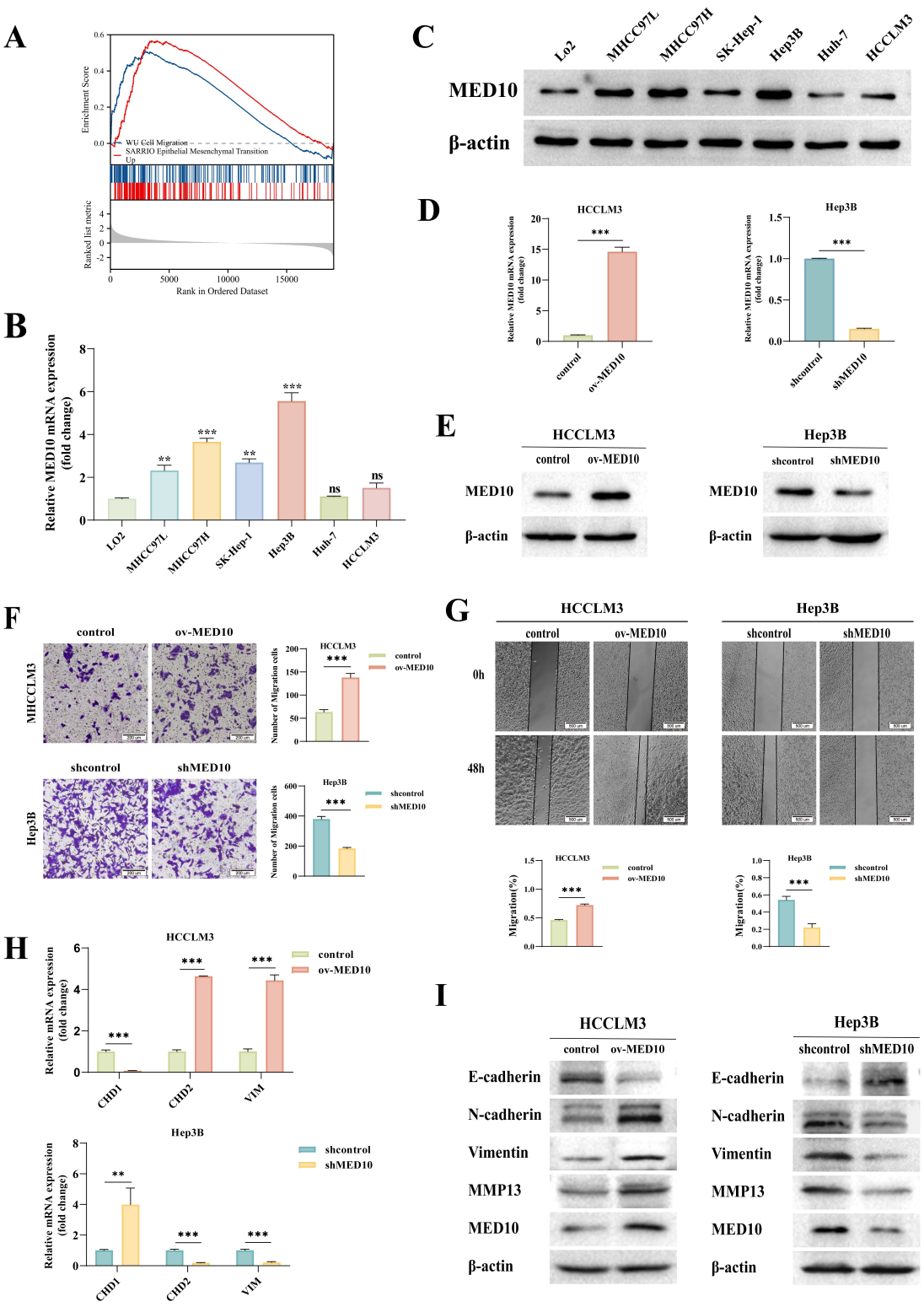

Fig. 2. MED10 promotes migration and EMT in HCC. (A) Gene Set Enrichment Analysis (GSEA) showing significant enrichment of cell migration and EMT pathways. (B,C) MED10 mRNA/protein expression in normal hepatocytes (LO2) versus HCC cell lines. (D,E) Validation of MED10 (over)expression (ov-MED10) and knockdown (shMED10) models. (F,G) Enhanced migration capacity after MED10 overexpression versus suppression in knockdown models (Transwell/wound-healing). Scale bars: 200 μm (F) and 500 μm (G). (H,I) EMT marker shifts: MED10 overexpression downregulated E-cadherin while upregulating N-cadherin, vimentin, and MMP13; knockdown reversed these effects. ns: $p \geq 0.05$; $^{**}p < 0.01$; $^{***}p < 0.001$.

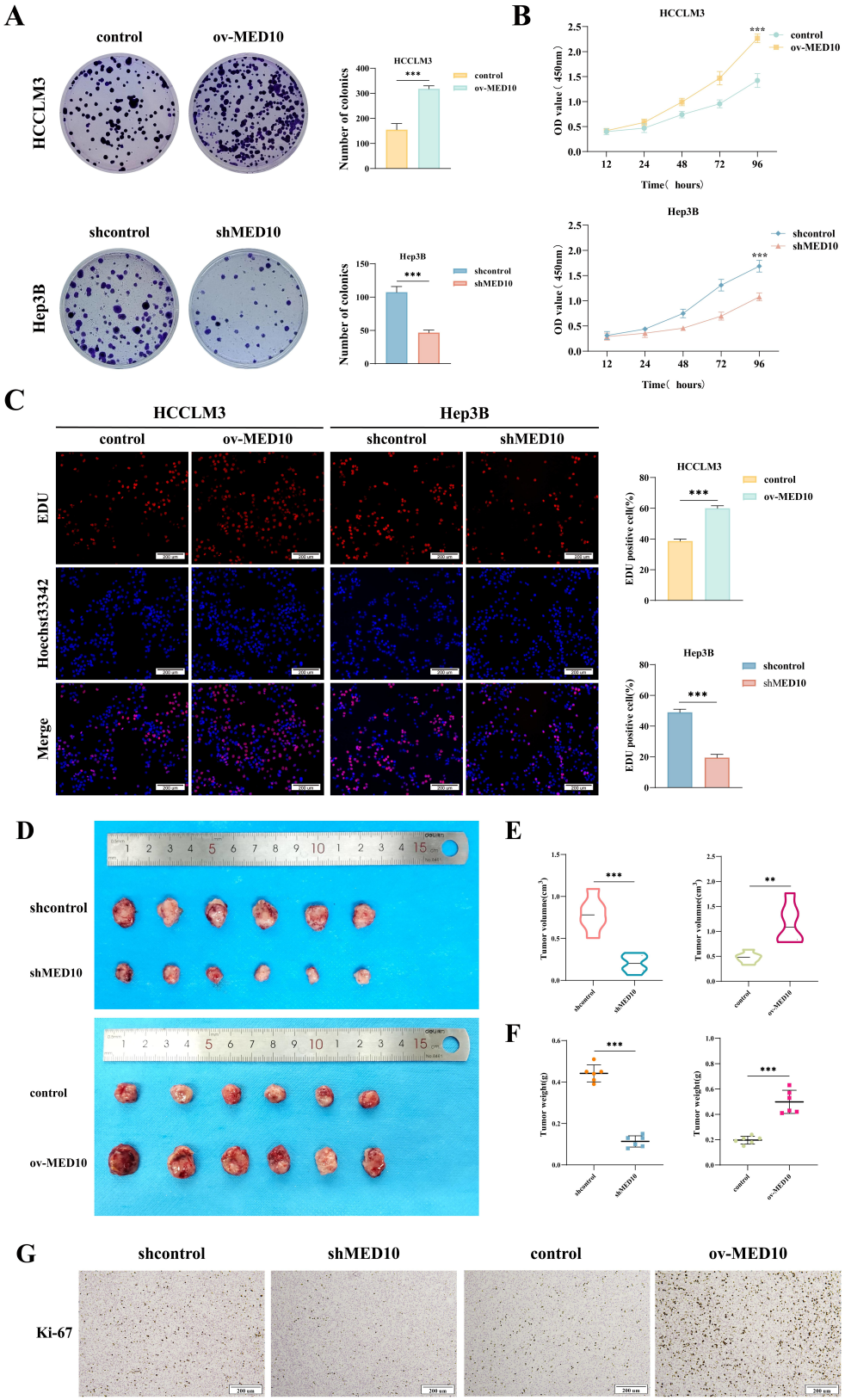

Fig. 3. MED10 promotes HCC cells proliferation. (A–C) Enhanced proliferative capacity in ov-MED10 cells versus suppression in shMED10 models across colony formation, CCK-8, and EdU assays. Scale bar = 200 μm. (D) Representative xenograft tumors from experimental groups post-excision (n = 6). (E,F) Significant reduction in tumor volume/weight in shMED10 cohort versus increased burden in ov-MED10 group relative to controls. (G) Immunohistochemical validation of proliferation marker Ki-67: diminished expression in shMED10 tumors versus intensified staining in ov-MED10 xenografts. Scale bar = 200 μm. $^{**}p < 0.01$; $^{***}p < 0.001$.

3.4 MED10 Regulates the Cell Cycle Progression of HCC Cells

To investigate MED10's role in proliferation, we analyzed TCGA data through functional enrichment. GO/KEGG pathway analysis revealed pronounced enrichment of MED10-correlated DEGs in cell cycle regulatory pathways (Fig. 4A). GSEA further implicated MED10 in proliferation and cell cycle processes including checkpoint control, G1/S transition, cyclin D1/CDK4 targets, cyclin D-associated G1 events, and RB1-mediated pathways (Fig. 4B). Protein-protein interaction network analysis (STRING) identified predicted binding partners CDK4, CDK6, CDK8, and CCNC (Fig. 4C). These findings establish MED10 as a regulator of cell cycle progression in HCC. Flow cytometry analysis revealed that MED10 overexpression in HCCLM3 cells significantly reduced G0/G1 phase occupancy while increasing S-phase fraction. Conversely, MED10 knockdown in Hep3B cells increased G0/G1 phase cells and decreased S-phase populations, with no significant G2/M phase alterations (Fig. 4D), indicating MED10's critical role in G1/S transition. Immunofluorescence of HCC tissues demonstrated co-localization of MED10 with key G1/S regulators CDK4, CDK6, and cyclin D1 (Fig. 4E). Western blotting confirmed MED10-dependent regulation: overexpression upregulated while knockdown suppressed CDK4, CDK6, and cyclin D1 expression (Fig. 4F). Taken together, MED10 enhances HCC proliferation by driving the G1/S cell cycle transition, possibly via regulation of CDK4, CDK6, and Cyclin D1.

3.5 MED10 Regulates Activation of the RAF/MEK/ERK/c-Myc Axis

To elucidate MED10's cell cycle regulatory mechanism, GSEA identified pronounced mitogen-activated protein Kinase (MAPK) pathway enrichment in high-expressing cohorts (Fig. 5A). Building on established MAPK/ERK functions in proliferation control [23], we interrogated pathway activity. Western blotting confirmed MED10 gain-of-function selectively enhanced RAF1-MEK-ERK cascade phosphorylation without affecting total protein abundance. Conversely, MED10 knockdown suppressed phosphorylation of these kinases (Fig. 5B), indicating MED10-dependent MAPK pathway activation. Since nuclear translocation of p-ERK1/2 is essential for transcriptional activation, immunofluorescence confirmed MED10's regulation of this process: nuclear p-ERK1/2 accumulation increased with MED10 overexpression and decreased upon knockdown (Fig. 5C). The transcription factor c-Myc, a key MAPK/ERK downstream effector, regulates cyclin and CDK transcription (e.g., CDK4, CDK6, cyclin D1) to control cell cycle progression [24,25]. GSEA linked MED10 to Myc pathway activation ("Myc active", "Myc targets up", "HCC up"; Fig. 5D), while TRRUST analysis confirmed c-Myc's enrichment in mitotic G1/S transition (Fig. 5E). Western blotting demonstrated MED10-dependent c-Myc regulation: overexpression upregulated and knockdown downregulated c-Myc expression (Fig. 5F). Integrated analysis of TRUST, CHEA, ENCODE, and ChIP Atlas databases predicted eight c-Myc target genes involved in G1/S control, including CDK4, CDK6, and CCND1 (Fig. 5G). JASPAR identified high-score c-Myc binding motifs in these genes' promoters (Fig. 5H). Collectively, these findings demonstrate that MED10 modulates both the RAF/MEK/ERK signaling pathway activation and c-Myc expression, potentially representing a key mechanism through which MED10 regulates cell cycle progression and proliferation in HCC cells.

3.6 MED10 Regulates Cell Cycle Progression by Modulating RAF1 Activation

To determine if MED10's pro-proliferative and cell cycle effects require MAPK signaling, we treated HCC cells with RAF inhibitor LY3009120. Proliferation assays (CCK-8, colony formation, EdU) demonstrated that MED10 overexpression-enhanced growth was partially reversed by LY3009120 (Fig. 6A–C). Flow cytometry confirmed MED10-mediated G0/G1 reduction and S-phase increase were similarly attenuated by RAF inhibition (Fig. 6D). Western blotting analysis revealed LY3009120 partially reversed MED10-driven phosphorylation of RAF1, MEK1/2, ERK1/2, and c-Myc (Fig. 6E), and correspondingly blunted MED10-induced upregulation of CDK4, CDK6, and cyclin D1 (Fig. 6F). Thus, MED10 regulates proliferation and cell cycle progression primarily through RAF, and related to MEK/ERK/c-Myc signaling. Conversely, MED10-promoted migration and EMT remained unaffected by RAF inhibition (**Supplementary Fig. 1A–C**), indicating these effects occur independently of MAPK pathway activation.

4. Discussion

Mediator complexes regulate gene expression at multiple stages of transcription, including preinitiation complex formation, transcriptional elongation, and mRNA splicing [26]. Growing evidence implicates dysregulation of Mediator complex subunits in cancer progression, where they play key roles in critical oncogenic processes such as migration, cell cycle, apoptosis, immune escape, tumor cell proliferation, and drug resistance [27–31]. As a critical subunit of the mediator complex, MED10 expression is markedly elevated in uterine fibroids, and facilitates tumor progression by enhancing proliferative capacity and metastatic potential through hsa-miR-590 regulation in bladder urothelial carcinoma [5,32]. Notably, recent studies have revealed that MED10 enhances cisplatin resistance in HCC by promoting PTEN ubiquitination, highlighting its significant potential as a therapeutic target. Our current study further uncovers a novel role of MED10 in HCC malignant progression and elucidates its underlying molecular mechanism [13]. In

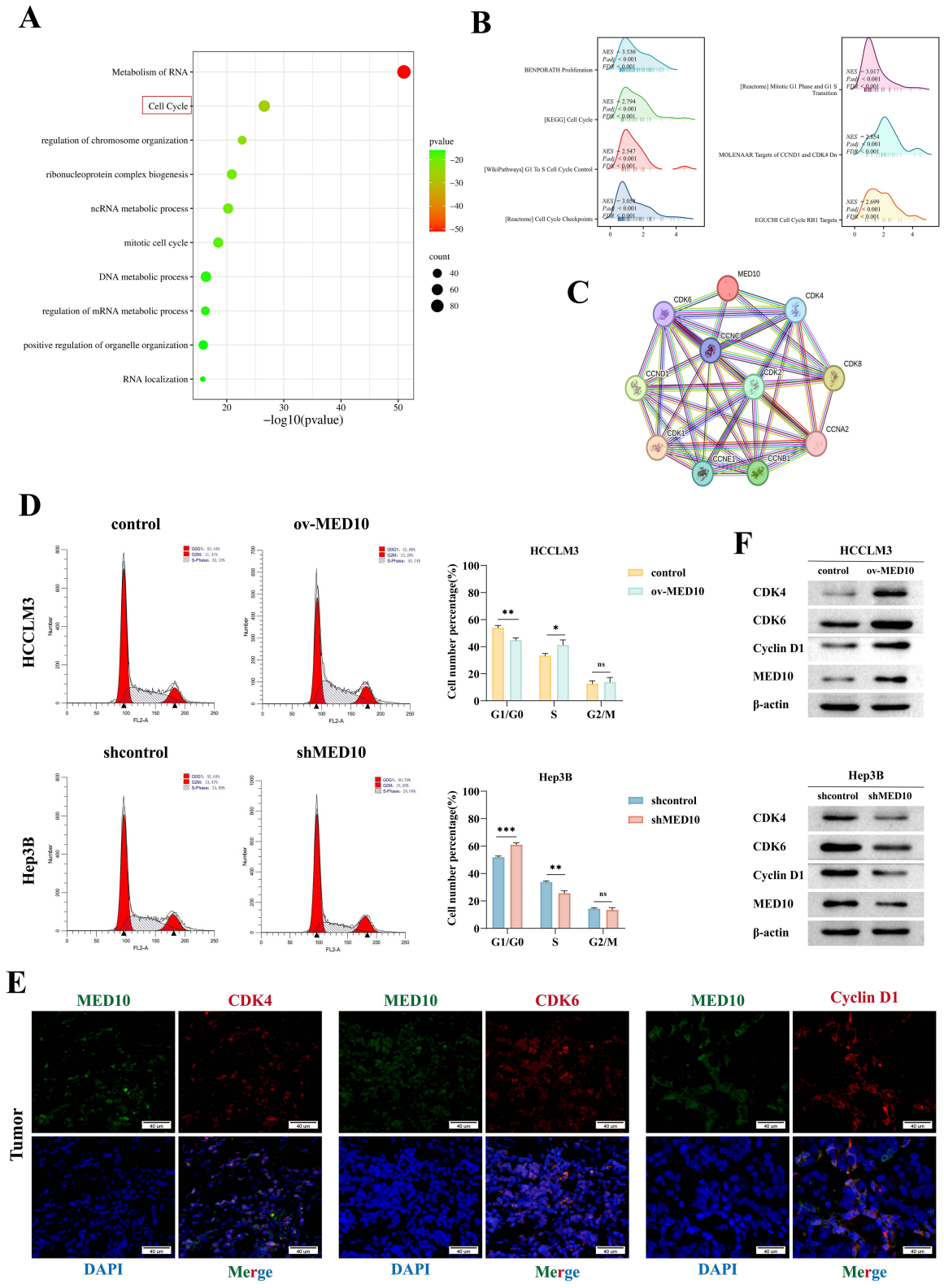

Fig. 4. MED10 orchestrates cell cycle progression in HCC. (A) Functional enrichment of MED10-associated genes (Gene Ontology (GO)/Kyoto Encyclopedia of Genes and Genomes (KEGG)) in TCGA-LIHC, such as cell cycle, etc. (B) GSEA of differentially expressed mRNAs stratified by MED10 expression. (C) Protein-protein interaction network linking MED10 to cell cycle regulators. (D) Flow cytometry quantification of cell cycle phase distribution following MED10 modulation. (E) Immunofluorescence co-localization of MED10 (green) with CDK4, CDK6, and cyclin D1 (red) in HCC tissues. Scale bar = 40 μm. (F) Western blotting analysis of CDK4/6 and cyclin D1 expression under MED10 modulation. ns: not significant ($p \geq 0.05$); *$p < 0.05$, **$p < 0.01$, ***$p < 0.001$.

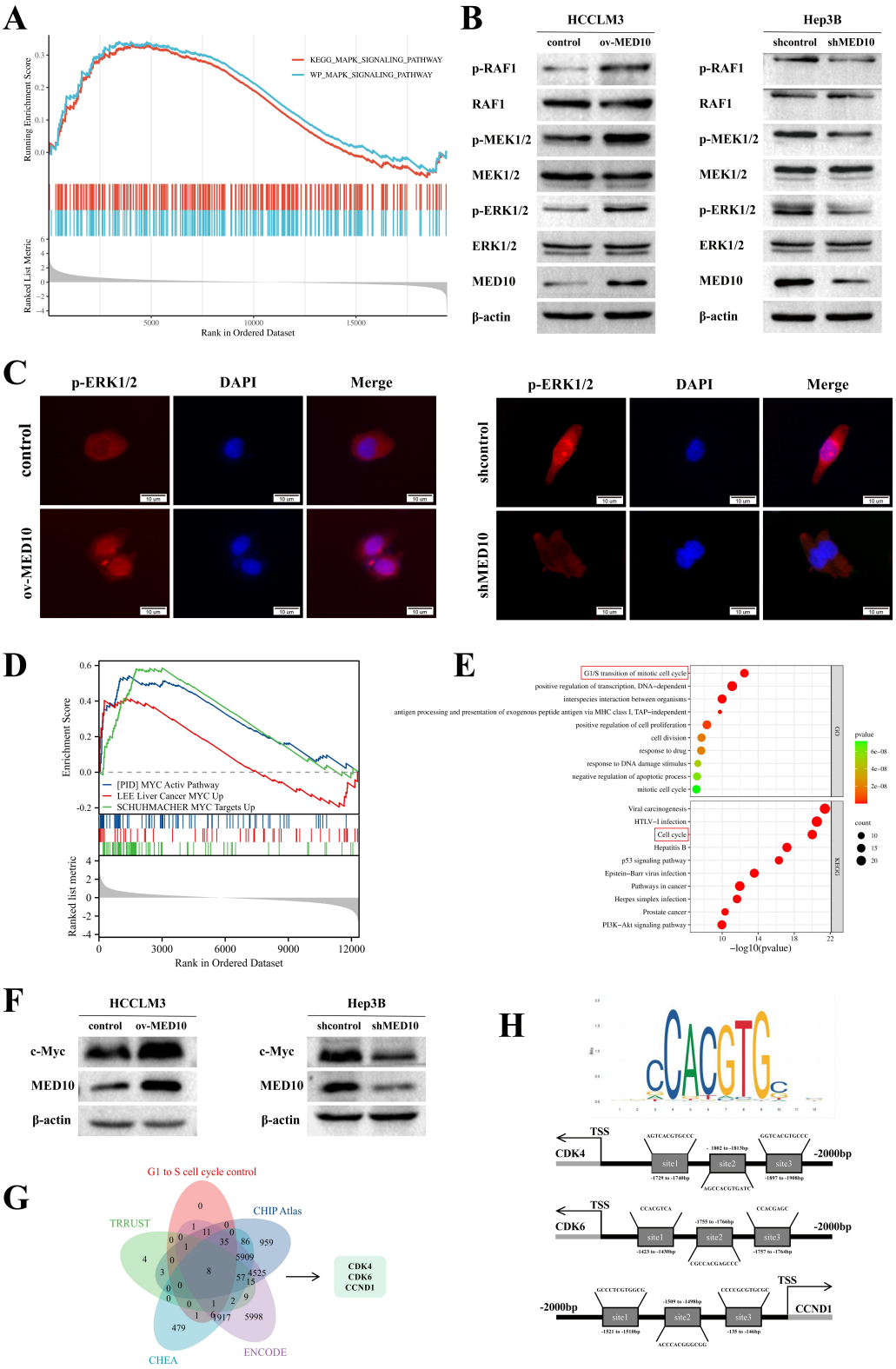

Fig. 5. MED10 regulates activation of the MAPK signaling axis. (A) GSEA linking MED10 to MAPK signaling. (B) Western blotting analysis of MAPK pathway components under MED10 modulation. (C) Subcellular localization of p-ERK1/2 by immunofluorescence. Scale bar = 10 μm. (D) GSEA enrichment of Myc-related pathways. (E) TRRUST-predicted c-Myc involvement in G1/S transition. (F) MED10-dependent c-Myc regulation via Western blotting. (G) Venn intersection of c-Myc target genes (TRUST/CHEA/ENCODE/ChIP Atlas) and G1/S regulators. (H) JASPAR-predicted c-Myc binding motifs in CDK4/CDK6/CCND1 promoters.

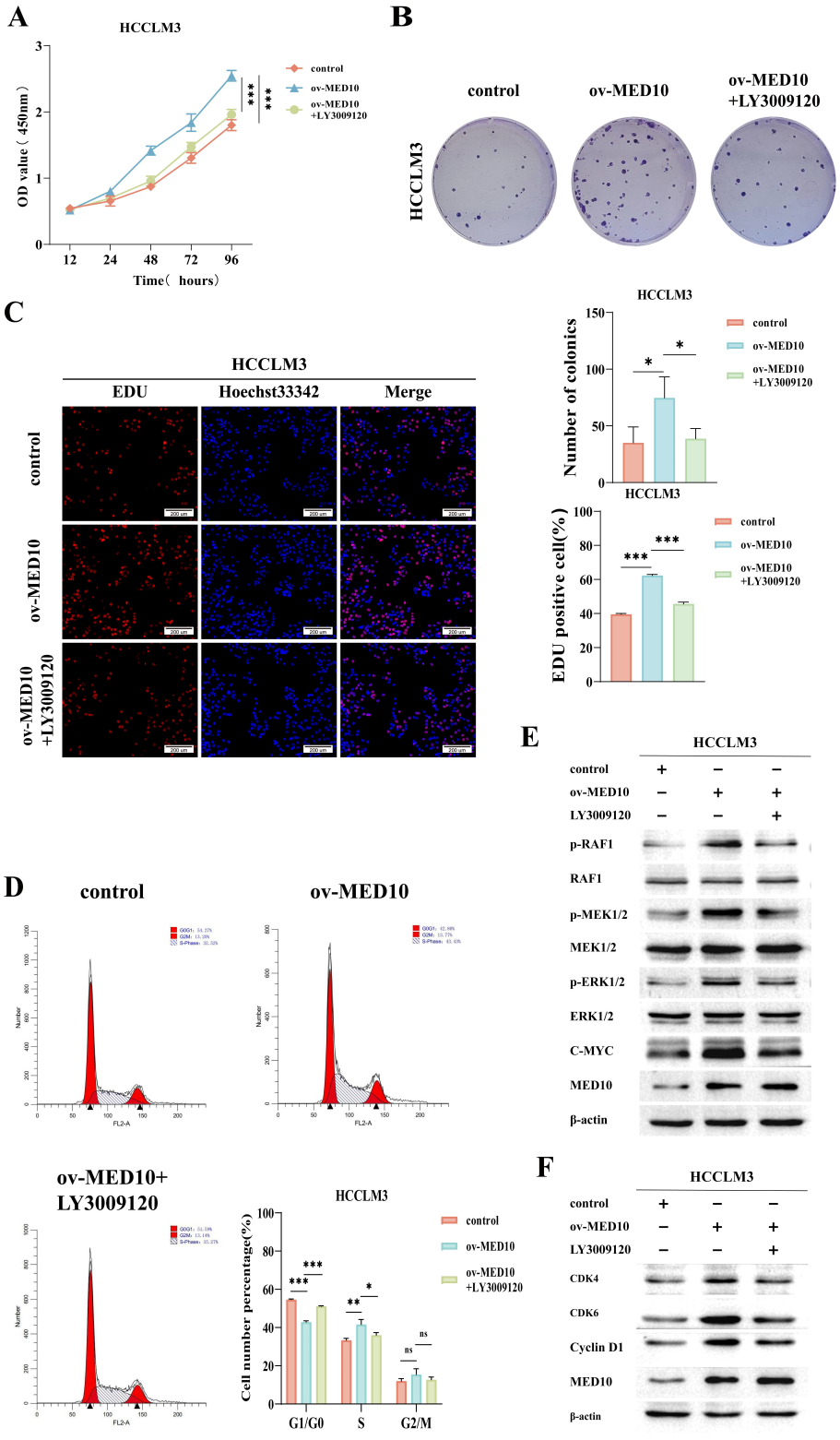

Fig. 6. RAF inhibition reverses MED10-driven proliferation and cell cycle progression in HCC. (A–C) CCK-8, colony formation, and EdU assays collectively demonstrated that the RAF inhibitor LY3009120 blocks MED10-driven proliferation. Scale bar = 200 μm. (D) Furthermore, flow cytometry analysis revealed that LY3009120 rescues the promoting effect of MED10 overexpression on cell cycle progression. (E) Western blotting assessed MAPK pathway protein expression following RAF1 phosphorylation inhibition in MED10-overexpressing HCCLM3 cells. (F) Additionally, Western blotting evaluated levels of cell cycle regulators CDK4, CDK6, and cyclin D1 in these cells after LY3009120 treatment. "ns" denotes $p \geq 0.05$; *$p < 0.05$, **$p < 0.01$, ***$p < 0.001$.

the present investigation, we observed that MED10 exhibits high expression levels in HCC and correlates with unfavorable patient prognosis. Moreover, MED10 was demonstrated to exert critical roles in HCC cell migration and the EMT, and modulated HCC cell cycle progression and proliferation through modulating RAF1 activation. Collectively, this study establishes a theoretical foundation for developing novel diagnostic and therapeutic strategies in HCC.

Elevated MED10 expression was observed in HCC tissues and correlated with poorer patient prognosis. Identified as an independent prognostic risk factor, MED10 formed the basis of a predictive nomogram demonstrating strong performance for HCC patient outcomes. These findings linking MED10 expression to survival and prognosis highlight its significant potential as both a prognostic biomarker and therapeutic target. Furthermore, MED10 levels showed significant associations with key clinical indicators of aggressiveness—including microvascular invasion, tumor thrombosis, larger tumor size, and advanced T stage—suggesting its involvement in HCC metastasis and proliferation.

The EMT represents a pivotal step in tumor invasion and early metastatic dissemination. Within tumor microenvironments, EMT activation drives tumor cell invasion and metastasis. GSEA findings revealed that cell migration and the EMT were significantly enriched in the patient cohort exhibiting high MED10 expression. Our findings reveal that elevated MED10 expression stimulates HCC cell migration and induces EMT, as evidenced by suppressed E-cadherin alongside enhanced N-cadherin and vimentin expression. Conversely, MED10 inhibition reversed this phenotypic shift. Furthermore, we observed a direct correlation between MED10 levels and MMP13 expression, a type I collagenase [33] implicated in extracellular matrix degradation and tumor metastasis. Collectively, these findings demonstrate that MED10 serves as a key regulator in HCC metastasis.

The capacity for uncontrolled proliferation represents a cardinal malignant trait of tumors, which is frequently linked to dysregulated cell cycle progression. GO, KEGG, and GSEA results revealed that MED10 is implicated in biological processes that include cell proliferation, cell cycle regulation, and control of the G1-to-S cell cycle transition. Notably, MED10 overexpression was shown to enhance HCC cell proliferation and facilitate the G1-to-S cell cycle phase transition. The knockdown of MED10 showed the opposite result. Cyclin D1 is the dominant cell cycle protein in the G1 phase. Upon complex formation with CDK4 or CDK6, cyclin D induces phosphorylation of the retinoblastoma protein (Rb), thereby enhancing E2F transcriptional activity. This cascade drives progression through the G1/S phase checkpoint, facilitating the rapid transition from G1 to S phase [34]. We found that the expression of CDK4, CDK6, and CCND1 increased after MED10 overexpression, and that the expression of these three genes was inhibited after MED10 knockdown.

The MAPK/ERK cascade represents one of the canonical pathways within the broader MAPK signaling network. Initiation of the RAS-to-ERK signaling cascade triggers downstream effector molecules, including transcription factors and kinases, which subsequently modulate gene expression patterns [23]. Ultimately, this process drives fundamental biological mechanisms in hepatocellular carcinoma (HCC), such as cell migration, proliferation, cell cycle progression, apoptosis, and drug resistance [35–37]. Enrichment analysis further established a significant association between MED10 and the MAPK signaling pathway. Notably, we demonstrated that MED10 regulates phosphorylation of the RAF1-MEK1/2-ERK1/2 cascade and facilitates nuclear translocation of p-ERK1/2. The nuclear translocation of activated ERK1/2 and the subsequent stimulation of downstream effector transcription factors are critical events enabling the MAPK signaling cascade to exert its functional outputs. We found that MED10 modulates c-Myc expression. As a critical transcription factor downstream of MAPK/ERK signaling, c-Myc drives expression of key cell cycle regulators including CDK6, CDK4, and cyclin D, ultimately facilitating G1/S phase transition [25,38]. Using a public database, we found that c-Myc is involved in regulation of the G1/S transition and is a common transcription factor for cyclin D, CDK4, and CDK6. Following RAF inhibitor LY3009120 treatment, phosphorylation of the RAF1-MEK-ERK cascade and c-Myc expression were suppressed, concomitantly reversing MED10-driven proliferation and cell cycle phenotypes.

Although widely utilized as a HCC biomarker for screening and clinical diagnosis, AFP exhibits undetectable elevation in nearly 30% of HCC cases, leading to suboptimal diagnostic sensitivity and specificity [39]. This diagnostic limitation underscores the need for novel biomarkers. Our findings identify dysregulated MED10 expression in HCC tissues that correlates with adverse clinical outcomes. Further, MED10 as a driver of HCC progression, accelerating tumor growth in both cellular models and living organisms, and interference with MED10 significantly inhibited tumor growth, which is mainly related to MED10 mediating activation of the MAPK/ERK axis to regulate the cell cycle process. Collectively, these data position MED10 as a dual-function target with diagnostic and therapeutic potential, establishing a conceptual framework for developing MED10-directed theranostic strategies. However, a paucity of drug development targeting MED10 as a therapeutic target and relevant clinical trials currently exist, necessitating further research to deeply explore the role and underlying mechanisms of MED10 in the malignant progression of HCC.

This work acknowledges certain limitations: while establishing MED10's association with adverse HCC outcomes, our conclusions derive primarily from retrospective analyses of public datasets and clinical cohorts. Fur-

thermore, information regarding the real-world follow-up of patients was lacking. Future studies should aim to enroll more subjects and conduct prospective clinical studies. Subjects should also be categorized according to population heterogeneity to further validate the potential of MED10 as a prognostic biomarker and its role in patients with HCC that have different genetic backgrounds and environmental factors. Secondly, our preliminary findings suggest that the regulatory effect The regulatory effects of MED10 on cell proliferation and cell cycle progression are dependent on its control of RAF1 activation. Nevertheless, we have yet to gain further insights into the mechanisms by which MED10 activates MAPK signaling axis. Therefore, future studies should continue to comprehensively explore the specific molecular mechanisms involved through additional experiments.

5. Conclusion

Collectively, this study furnishes multidimensional evidence that highlights the functional significance of MED10 in HCC pathogenesis, as well as its potential utility as a prognostic biomarker for HCC disease progression. Our findings demonstrated that MED10 exerts critical functional roles in key biological processes, including HCC cell migration, the EMT, cell proliferation, and cell cycle regulation. Mechanistically, MED10 primarily regulates proliferation and cell cycle progression by promoting RAF1 activation, a process possibly associated with MEK/ERK signaling and c-Myc expression. These findings collectively offer promising molecular targets for the development of HCC-directed anticancer therapeutic strategies.

Availability of Data and Materials

All data reported in this paper will be shared by the corresponding author upon reasonable request.

Author Contributions

JHL and YXL: validation, formal analysis, investigation, visualization, writing - original Draft, writing - review & editing. KJL: validation, investigation, methodology. ZQL: validation, investigation. BDC: investigation, resources, formal analysis. YB: conceptualization, methodology, supervision, project administration, funding, acquisition, writing - review & editing. All authors contributed to editorial changes in the manuscript. All authors read and approved the final manuscript. All authors have participated sufficiently in the work and agreed to be accountable for all aspects of the work.

Ethics Approval and Consent to Participate

The clinical research protocol was conducted in full compliance with the ethical principles of the Declaration of Helsinki. Written informed consent was obtained from all human participants or their legally authorized representatives prior to study enrollment. All animal experiments were performed in strict compliance with the guidelines established by Animal Welfare Act and Ningxia Medical University. The studies involving human participants and animal experimental protocol were reviewed and approved by the Medical Ethics Review Committee of Ningxia Medical University (Approval No. 2025-N092).

Acknowledgment

Not applicable.

Funding

This work was supported by the National Natural Science Foundation of China [grant numbers 81960533], Ningxia natural science foundation [grant numbers 2023AAC03606], Ningxia natural science foundation [grant numbers 2023AAC03507], School-level scientific research project of Ningxia Medical University [grant numbers XM2022041], 2024 First-class Discipline Funding of Ningxia Medical University (Third Clinical College of Medicine) [grant numbers 4301240006], Key R&D Program Talent Introduction Special Project of Ningxia Hui Autonomous Region (2024BEH04154).

Conflict of Interest

The authors declare no conflict of interest.

Supplementary Material

Supplementary material associated with this article can be found, in the online version, at https://doi.org/10.31083/FBL39944.

References

[1] Sankar K, Gong J, Osipov A, Miles SA, Kosari K, Nissen NN, *et al*. Recent advances in the management of hepatocellular carcinoma. Clinical and Molecular Hepatology. 2024; 30: 1–15. https://doi.org/10.3350/cmh.2023.0125.

[2] Lindblad KE, Ruiz de Galarreta M, Lujambio A. Tumor-Intrinsic Mechanisms Regulating Immune Exclusion in Liver Cancers. Frontiers in Immunology. 2021; 12: 642958. https://doi.org/10.3389/fimmu.2021.642958.

[3] He K, Xie M, Hong W, Li Y, Yin Y, Gao X, *et al*. CENPL accelerates cell proliferation, cell cycle, apoptosis, and glycolysis via the MEK1/2-ERK1/2 pathway in hepatocellular carcinoma. The International Journal of Biochemistry & Cell Biology. 2024; 166: 106481. https://doi.org/10.1016/j.biocel.2023.106481.

[4] Yan T, Yu L, Zhang N, Peng C, Su G, Jing Y, *et al*. The advanced development of molecular targeted therapy for hepatocellular carcinoma. Cancer Biology & Medicine. 2022; 19: 802–817. https://doi.org/10.20892/j.issn.2095-3941.2021.0661.

[5] Wu CC, Wang YH, Hu SW, Wu WL, Yeh CT, Bamodu OA. MED10 Drives the Oncogenicity and Refractory Phenotype of Bladder Urothelial Carcinoma Through the Upregulation of hsa-miR-590. Frontiers in Oncology. 2022; 11: 744937. https://doi.org/10.3389/fonc.2021.744937.

[6] Li X, Yiliyaer N, Guo T, Zhao H, Lei Y, Gu S. The indispensable role of Mediator complex subunit 27 during neurodevelop-

ment. Cell & Bioscience. 2025; 15: 83. https://doi.org/10.1186/s13578-025-01425-7.

[7] Zhang X, Zhang M, Sun H, Wang X, Wang X, Sheng W, *et al*. The role of transcription factors in the crosstalk between cancer-associated fibroblasts and tumor cells. Journal of Advanced Research. 2025; 67: 121–132. https://doi.org/10.1016/j.jare.2024.01.033.

[8] Li Z, Sun M, Yang R, Wang Z, Zhu Q, Zhang Y, *et al*. Mediator complex subunit 1 promotes oral squamous cell carcinoma progression by activating MMP9 transcription and suppressing $CD8^+$ T cell antitumor immunity. Journal of Experimental & Clinical Cancer Research. 2024; 43: 270. https://doi.org/10.1186/s13046-024-03191-9.

[9] Shen Y, Zhou L, Xu M, Tan Z, Yao K, Wang W. MED1 induces M2 polarization of tumor-associated macrophages to aggravate breast cancer. Genes & Genomics. 2023; 45: 1517–1525. https://doi.org/10.1007/s13258-023-01435-0.

[10] Zuberi A, Huang Y, Dotts AJ, Wei H, Coon JS, 5th, Liu S, *et al*. MED12 mutation activates the tryptophan/kynurenine/AHR pathway to promote growth of uterine leiomyomas. JCI Insight. 2023; 8: e171305. https://doi.org/10.1172/jci.insight.171305.

[11] Yang W, Gao K, Qian Y, Huang Y, Xiang Q, Chen C, *et al*. A novel tRNA-derived fragment AS-tDR-007333 promotes the malignancy of NSCLC via the HSPB1/MED29 and ELK4/MED29 axes. Journal of Hematology & Oncology. 2022; 15: 53. https://doi.org/10.1186/s13045-022-01270-y.

[12] Li H, Li K, Shu D, Shen M, Tan Z, Zhang W, *et al*. MED16 Promotes Tumour Progression and Tamoxifen Sensitivity by Modulating Autophagy through the mTOR Signalling Pathway in ER-Positive Breast Cancer. Life. 2022; 12: 1461. https://doi.org/10.3390/life12101461.

[13] Cai Q, Liu J, Xiao J, Chen J, Lv L, Yang F. MED10 Increases Cisplatin Resistance by Promoting PTEN Ubiquitination of Hepatocellular Carcinoma. Current Cancer Drug Targets. 2025. https://doi.org/10.2174/0115680096330893241221141235. (in press)

[14] Li T, Fu J, Zeng Z, Cohen D, Li J, Chen Q, *et al*. TIMER2.0 for analysis of tumor-infiltrating immune cells. Nucleic Acids Research. 2020; 48: W509–W514. https://doi.org/10.1093/nar/gkaa407.

[15] Yu G, Wang LG, Han Y, He QY. clusterProfiler: an R package for comparing biological themes among gene clusters. Omics: a Journal of Integrative Biology. 2012; 16: 284–287. https://doi.org/10.1089/omi.2011.0118.

[16] Zhou Y, Zhou B, Pache L, Chang M, Khodabakhshi AH, Tanaseichuk O, *et al*. Metascape provides a biologist-oriented resource for the analysis of systems-level datasets. Nature Communications. 2019; 10: 1523. https://doi.org/10.1038/s41467-019-09234-6.

[17] Szklarczyk D, Gable AL, Nastou KC, Lyon D, Kirsch R, Pyysalo S, *et al*. The STRING database in 2021: customizable protein-protein networks, and functional characterization of user-uploaded gene/measurement sets. Nucleic Acids Research. 2021; 49: D605–D612. https://doi.org/10.1093/nar/gkaa1074.

[18] Han H, Cho JW, Lee S, Yun A, Kim H, Bae D, *et al*. TRRUST v2: an expanded reference database of human and mouse transcriptional regulatory interactions. Nucleic Acids Research. 2018; 46: D380–D386. https://doi.org/10.1093/nar/gkx1013.

[19] Keenan AB, Torre D, Lachmann A, Leong AK, Wojciechowicz ML, Utti V, *et al*. ChEA3: transcription factor enrichment analysis by orthogonal omics integration. Nucleic Acids Research. 2019; 47: W212–W224. https://doi.org/10.1093/nar/gkz446.

[20] Zou Z, Ohta T, Miura F, Oki S. ChIP-Atlas 2021 update: a data-mining suite for exploring epigenomic landscapes by fully integrating ChIP-seq, ATAC-seq and Bisulfite-seq data. Nucleic Acids Research. 2022; 50: W175–W182. https://doi.org/10.1093/nar/gkac199.

[21] Rosenbloom KR, Dreszer TR, Long JC, Malladi VS, Sloan CA, Raney BJ, *et al*. ENCODE whole-genome data in the UCSC Genome Browser: update 2012. Nucleic Acids Research. 2012; 40: D912–D917. https://doi.org/10.1093/nar/gkr1012.

[22] Mathelier A, Zhao X, Zhang AW, Parcy F, Worsley-Hunt R, Arenillas DJ, *et al*. JASPAR 2014: an extensively expanded and updated open-access database of transcription factor binding profiles. Nucleic Acids Research. 2014; 42: D142–D147. https://doi.org/10.1093/nar/gkt997.

[23] Song YJ, Kim JE, Rajbongshi L, Lim YS, Ok YJ, Hwang SY, *et al*. Silencing of Epidermal Growth Factor-like Domain 8 Promotes Proliferation and Cancer Aggressiveness in Human Ovarian Cancer Cells by Activating ERK/MAPK Signaling Cascades. International Journal of Molecular Sciences. 2025; 26: 274. https://doi.org/10.3390/ijms26010274.

[24] Liu J, Wang S, Zhang C, Wei Z, Han D, Song Y, *et al*. Anillin contributes to prostate cancer progression through the regulation of IGF2BP1 to promote c-Myc and MAPK signaling. American Journal of Cancer Research. 2024; 14: 490–506. https://doi.org/10.62347/UYQH7683.

[25] Li HL, Dong LL, Jin MJ, Li QY, Wang X, Jia MQ, *et al*. A Review of the Regulatory Mechanisms of N-Myc on Cell Cycle. Molecules. 2023; 28: 1141. https://doi.org/10.3390/molecules28031141.

[26] Kolonay DW, Grueter CE, Baskin KK. Differential regulation during development, aging, and disease implies heart cell specific functions of the Mediator Complex. Journal of Molecular and Cellular Cardiology Plus. 2025; 12: 100456. https://doi.org/10.1016/j.jmccpl.2025.100456.

[27] Guzman J, Hart M, Weigelt K, Neumann A, Aigner A, Andolfi C, *et al*. The MicroRNA miR-454 and the mediator complex component MED12 are regulators of the androgen receptor pathway in prostate cancer. Scientific Reports. 2025; 15: 10272. https://doi.org/10.1038/s41598-025-95250-0.

[28] Ouyang B, Bi M, Jadhao M, Bick G, Zhang X. miR-205 Regulates Tamoxifen Resistance by Targeting Estrogen Receptor Coactivator MED1 in Human Breast Cancer. Cancers. 2024; 16: 3992. https://doi.org/10.3390/cancers16233992.

[29] Bhole R, Shinkar J, Labhade S, Karwa P, Kapare H. MED12 dysregulation: insights into cancer and therapeutic resistance. Naunyn-Schmiedeberg's Archives of Pharmacology. 2025; 398: 10049–10069. https://doi.org/10.1007/s00210-025-04006-0.

[30] Jin X, Zhang Y, Hu W, Liu C, Cai D, Sun J, *et al*. Developing a prognostic model for hepatocellular carcinoma based on MED19 and clinical stage and determining MED19 as a therapeutic target. Journal of Cancer Research and Clinical Oncology. 2024; 150: 446. https://doi.org/10.1007/s00432-024-05978-x.

[31] Fu X, Liu S, Cao D, Li C, Ji H, Wang G. Med23 deficiency reprograms the tumor microenvironment to promote lung tumorigenesis. British Journal of Cancer. 2024; 130: 716–727. https://doi.org/10.1038/s41416-023-02556-9.

[32] Sahar T, Nigam A, Anjum S, Waziri F, Biswas S, Jain SK, *et al*. Interactome Analysis of the Differentially Expressed Proteins in Uterine Leiomyoma. Anti-cancer Agents in Medicinal Chemistry. 2019; 19: 1293–1312. https://doi.org/10.2174/1871520619666190206143523.

[33] Ho HY, Chen MK, Lin CC, Lo YS, Chuang YC, Hsieh MJ. Epiberberine suppresses the metastasis of head and neck squamous cell carcinoma cells by regulating the MMP-13 and JNK pathway. Journal of Cellular and Molecular Medicine. 2023; 27: 3796–3804. https://doi.org/10.1111/jcmm.17954.

[34] Koirala N, Dey N, Aske J, De P. Targeting Cell Cycle Progression in HER2+ Breast Cancer: An Emerging Treatment Opportunity. International Journal of Molecular Sciences. 2022; 23: 6547. https://doi.org/10.3390/ijms23126547.

[35] Huang K, Liu Z, Xie Z, Li X, Zhang H, Chen Y, *et al*. HIGD2A silencing impairs hepatocellular carcinoma growth via inhibiting mitochondrial function and the MAPK/ERK pathway. Journal of Translational Medicine. 2023; 21: 253. https://doi.org/10.1186/s12967-023-04105-7.

[36] Yang J, Li S, He J, Xu Q, Xie M, Yang C, *et al*. Dual role of PID1 in regulating apoptosis induced by distinct anticancer-agents through AKT/Raf-1-dependent pathway in hepatocellular carcinoma. Cell Death Discovery. 2023; 9: 139. https://doi.org/10.1038/s41420-023-01405-1.

[37] Yuan J, Lv T, Yang J, Wu Z, Yan L, Yang J, *et al*. HDLBP Promotes Hepatocellular Carcinoma Proliferation and Sorafenib Resistance by Suppressing Trim71-dependent RAF1 Degradation. Cellular and Molecular Gastroenterology and Hepatology. 2023; 15: 307–325. https://doi.org/10.1016/j.jcmgh.2022.10.005.

[38] Othman NS, Mohd Azman DK. Andrographolide Induces G2/M Cell Cycle Arrest and Apoptosis in Human Glioblastoma DBTRG-05MG Cell Line via ERK1/2 /c-Myc/p53 Signaling Pathway. Molecules. 2022; 27: 6686. https://doi.org/10.3390/molecules27196686.

[39] Zhao K, Zhou X, Xiao Y, Wang Y, Wen L. Research Progress in Alpha-fetoprotein-induced Immunosuppression of Liver Cancer. Mini Reviews in Medicinal Chemistry. 2022; 22: 2237–2243. https://doi.org/10.2174/1389557522666220218124816.